



## ATLAS Paper Draft

---

### Search for supersymmetry in final states with two same-sign or three leptons and jets using $\sqrt{s} = 13$ TeV $pp$ collision data collected with the ATLAS detector

SUSY-2016-14

Version: 0.0

To be submitted to:

---

**Comments are due by:** Comments deadline

---

#### Abstract

A search for strongly produced supersymmetric particles using signatures involving multiple energetic jets and either two isolated same-sign leptons ( $e$  or  $\mu$ ) or at least three isolated leptons is presented. The analysis relies also on  $b$ -tagged jets or missing transverse momentum, to extend its sensitivity. A data sample of proton–proton collisions at  $\sqrt{s} = 13$  TeV recorded with the ATLAS detector at the Large Hadron Collider in 2015 and 2016, corresponding to a total integrated luminosity of **[36.5 UPDATE]** fb<sup>−1</sup>, is used for the search. No significant excess over the Standard Model expectation is observed. The results are interpreted in several simplified supersymmetric models featuring  $R$ -parity conservation and  $R$ -parity violation, extending the exclusion limits from previous searches. In these models, gluino masses are excluded at 95% confidence level up to **[UPDATE]** TeV and bottom squark masses are also excluded up to **[UPDATE]** GeV for light neutralinos.

---

### **Analysis Team**

[*email:* atlas-susy-2016-14-editors@cern.ch]

B. Abbott, J.-F. Arguin, S. Berlendis, G. Carrillo-Montoya, F. Cardillo,  
A. Di Simone, O. Ducu, Z.D. Greenwood, G. Herten, D. Jana, Y. Liu, A. Lleres,  
J. Maurer, S. Mete, A. Paramonov, J. Poveda, P. Pralavorio, H. Ren, O. Rifki,  
C. Sandoval, Y.-T. Shen, P. Skubic, A. Soffa, A. Taffard, P. Tornambé, C. Walker,  
X. Zhuang

---

### **Editorial Board**

[*email:* atlas-susy-2016-14-editorial-board@cern.ch]

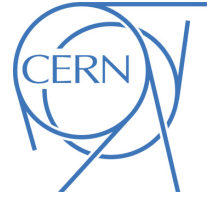
Jamie Boyd (chair), Sara Strandberg, Kerim Suruliz

---



# ATLAS Paper

SUSY-2016-14



Draft version 0.0

## Search for supersymmetry in final states with two same-sign or three leptons and jets using $\sqrt{s} = 13$ TeV $pp$ collision data collected with the ATLAS detector

The ATLAS Collaboration

16th February 2017

A search for strongly produced supersymmetric particles using signatures involving multiple energetic jets and either two isolated same-sign leptons ( $e$  or  $\mu$ ) or at least three isolated leptons is presented. The analysis relies also on  $b$ -tagged jets or missing transverse momentum, to extend its sensitivity. A data sample of proton–proton collisions at  $\sqrt{s} = 13$  TeV recorded with the ATLAS detector at the Large Hadron Collider in 2015 and 2016, corresponding to a total integrated luminosity of  $[36.5 \text{ UPDATE}] \text{fb}^{-1}$ , is used for the search. No significant excess over the Standard Model expectation is observed. The results are interpreted in several simplified supersymmetric models featuring  $R$ -parity conservation and  $R$ -parity violation, extending the exclusion limits from previous searches. In these models, gluino masses are excluded at 95% confidence level up to  $[\text{UPDATE}]$  TeV and bottom squark masses are also excluded up to  $[\text{UPDATE}]$  GeV for light neutralinos.

## Contents

<b>1</b>	<b>Introduction</b>	<b>4</b>
<b>2</b>	<b>The ATLAS detector</b>	<b>6</b>
<b>3</b>	<b>Dataset and simulated event samples</b>	<b>7</b>
<b>4</b>	<b>Event selection</b>	<b>9</b>
<b>5</b>	<b>Background estimation</b>	<b>11</b>
5.1	Detector background estimation methods	11
5.2	Validation of background estimates	12
<b>6</b>	<b>Systematic uncertainties on the background estimation</b>	<b>13</b>
<b>7</b>	<b>Results, interpretation and limits</b>	<b>15</b>
<b>8</b>	<b>Conclusion</b>	<b>22</b>
	<b>Appendix</b>	<b>28</b>

## 1 Introduction

Supersymmetry (SUSY) [1–6] is one of the most popular extension of the Standard Model (SM); a general review can be found in Ref. [7]. In its minimal realisation (the MSSM) [8, 9] it predicts a new bosonic (fermionic) partner for each fundamental SM fermion (boson), as well as an additional Higgs doublet. If  $R$ -parity is conserved (RPC) [10] the lightest supersymmetric particle (LSP) is stable and is typically the lightest neutralino<sup>1</sup>  $\tilde{\chi}_1^0$ . In many models, the LSP can be a viable dark matter candidate [11, 12] and produce collider signatures with large missing transverse momentum at the Large Hadron Collider (LHC). On the contrary, if  $R$ -parity is violated (RPV) [10], high jet and lepton multiplicity events are expected at the LHC. Both RPC and RPV scenarios can match the two same-sign or three leptons and jets signature considered in this paper.

In order to address the SM hierarchy problem with SUSY models [13–16], TeV-scale masses are required [17, 18] for the partners of the gluons (gluinos  $\tilde{g}$ ) and of the top quark chiral degrees of freedom (top squarks  $\tilde{t}_L$  and  $\tilde{t}_R$ ), due to the large top Yukawa coupling<sup>2</sup>. The latter also favours significant  $\tilde{t}_L$ – $\tilde{t}_R$  mixing, so that the lighter mass eigenstate  $\tilde{t}_1$  is in many scenarios lighter than the other squarks [19, 20]. Bottom squarks ( $\tilde{b}$ ) may also be light, being bound to top squarks by  $SU(2)_L$  invariance. This leads to potentially large production cross-sections for gluino pairs ( $\tilde{g}\tilde{g}$ ), top–antitop squark pairs ( $\tilde{t}_1\tilde{t}_1^*$ ) and bottom–antibottom squark pairs ( $\tilde{b}_1\tilde{b}_1^*$ ) at the LHC [21]. Production of isolated leptons may arise in the cascade decays of those superpartners to SM quarks and neutralinos  $\tilde{\chi}_1^0$ , via intermediate neutralinos  $\tilde{\chi}_{2,3,4}^0$ .

<sup>1</sup> The SUSY partners of the Higgs and electroweak gauge bosons mix to form the mass eigenstates known as charginos ( $\tilde{\chi}_l^\pm$ ,  $l = 1, 2$  ordered by increasing mass) and neutralinos ( $\tilde{\chi}_m^0$ ,  $m = 1, \dots, 4$  ordered by increasing mass).

<sup>2</sup> The partners of the left-handed (right-handed) quarks are labelled  $\tilde{q}_{L(R)}$ . In the case where there is significant  $L/R$  mixing (as is the case for third generation squarks) the mass eigenstates of these squarks are labelled  $\tilde{q}_{1,2}$  ordered in increasing mass.

or charginos  $\tilde{\chi}_{1,2}^\pm$  that in turn lead to  $W$ ,  $Z$  or Higgs bosons, or to lepton superpartners (sleptons). Lighter third-generation squarks would also enhance  $\tilde{g} \rightarrow t\tilde{t}_1^*$  or  $\tilde{g} \rightarrow b\tilde{b}_1^*$  branching ratios over the generic decays involving light-flavour squarks, favouring the production of heavy flavour quarks and, in the case of top quarks, additional leptons.

This paper presents a search for SUSY in final states with two leptons (electrons or muons) of the same electric charge (referred to as same-sign (SS) leptons) or three leptons (3L) in any charge combination, jets and in some cases also missing transverse momentum (whose magnitude is referred to as  $E_T^{\text{miss}}$ ). It is an extension of an earlier search performed by ATLAS with  $\sqrt{s} = 13$  TeV data [22], and uses the data collected by the ATLAS experiment [23] in proton–proton ( $pp$ ) collisions during 2015 and 2016. A similar search for SUSY in this topology was also performed by the CMS Collaboration at  $\sqrt{s} = 13$  TeV [24]. While the same-sign leptons signature is present in many scenarios of physics beyond the SM (BSM), SM processes leading to such final states have very small cross-sections. Compared to other BSM searches, analyses based on same-sign leptons therefore allow the use of looser kinematic requirements (for example, on  $E_T^{\text{miss}}$  or the momentum of jets and leptons), preserving sensitivity to scenarios with small mass differences between gluinos/squarks and the LSP, or in which  $R$ -parity is not conserved.

The sensitivity to a wide range of models is illustrated by the interpretation of the results in the context of twelve different SUSY simplified models [25–27] that may lead to same-sign or three-lepton signatures. For RPC models, the first four scenarios focus on gluino pair production with generic decays into on-shell (Fig. 1(a)) or off-shell (Fig. 1(b)) top quarks or light quarks. The latter are accompanied by a cascade involving a  $\tilde{\chi}_1^\pm$  and a  $\tilde{\chi}_2^0$  (Fig. 1(c)) or a  $\tilde{\chi}_2^0$  and light sleptons and sneutrinos (Fig. 1(d)). The other two RPC scenarios target the direct production of third generation squark pairs with subsequent electroweakino-mediation (Fig. 1(e) and 1(f)). The former is a generic same-sign lepton search for bottom squark. The latter, addressed here by looking for a three lepton same-sign final state, is a tentative model that could explain the excesses seen in same-sign signatures during Run1 [28]. Finally, a low fine-tuned generic SUSY model, the non-universal Higgs model with two extra parameters (NUHM2) [29, 30], is also considered.

In the case of non-zero RPV couplings in the baryonic sector ( $\lambda''_{ijk} \neq 0$ ), as proposed in Minimal Flavor Violation scenarios [31–33], gluino and squarks may decay directly to top quarks, leading to final states with same-sign leptons [34, 35] and  $b$ -tagged jets (Figs. 1(g), 1(h)). Alternatively gluino decay to neutralino LSP, that further decays to SM particle via  $\lambda'$  or  $\lambda''$ , is also possible (Figs. 1(i), 1(j)). Due to the absence of neutralinos in the final state, lower  $E_T^{\text{miss}}$  from the neutrinos produced in the top quark decays is expected in these scenarios. Pair-production of right-handed<sup>3</sup> like-sign down squarks (Figs. 1(k), 1(l)) are also considered in this paper. In all of these scenarios, antisquarks decay into the charge-conjugate final states of those indicated for the corresponding squarks, and gluinos decay with equal probabilities into a certain final state or its charge conjugate.

After describing the experimental apparatus (Section 2) and the simulated event samples (Section 3), the nineteen signal regions (SRs) designed to achieve good sensitivity for twelve SUSY scenarios are presented (Section 4). Section 5 describes the estimation of the contribution from SM processes to the signal regions, validated by comparisons with data in dedicated regions. The results are presented in Section 7 together with the statistical procedure used to interpret the results in the context of the SUSY benchmark scenarios. Finally, Section 8 summarises the main conclusions of this paper.

<sup>3</sup> These RPV baryon-number-violating couplings only couple to  $SU(2)$  singlets.

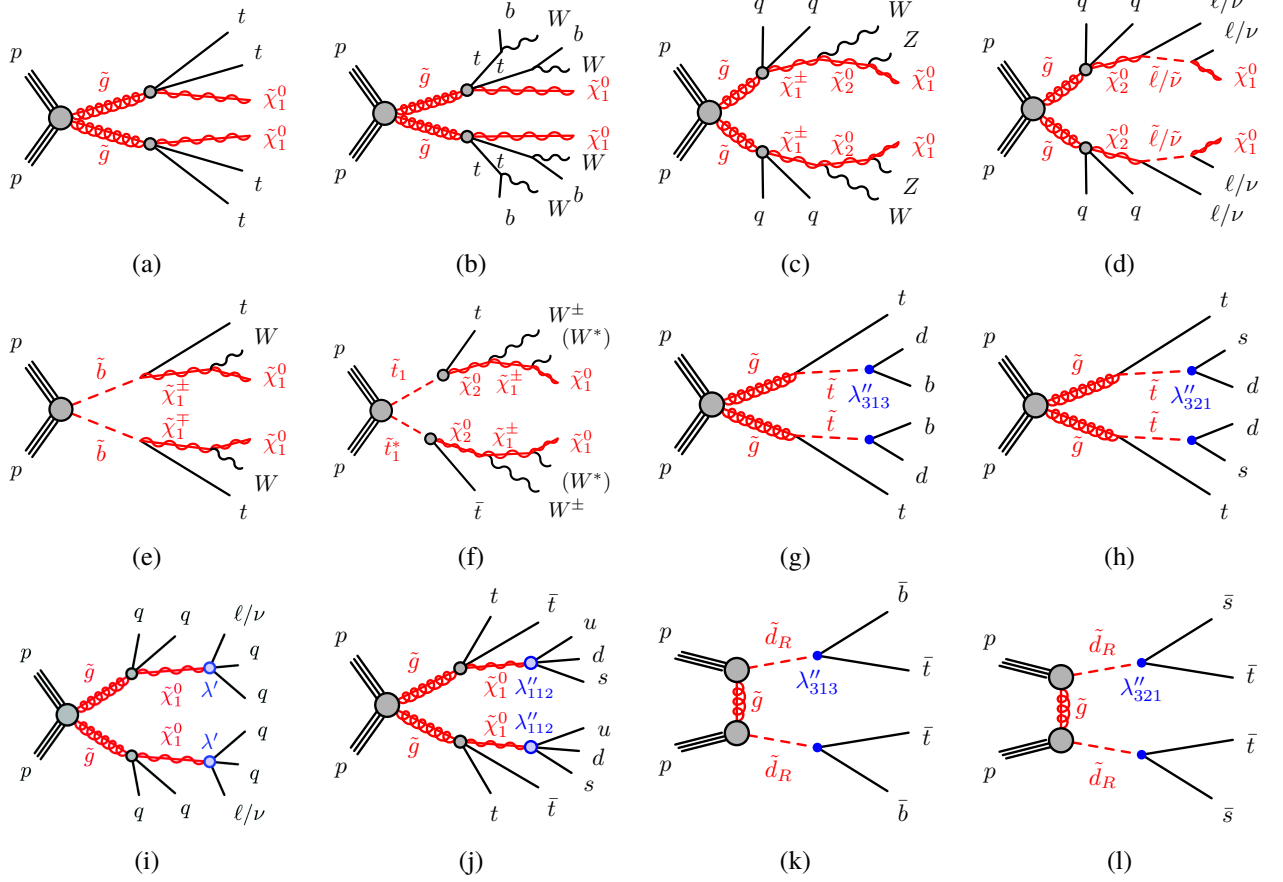


Figure 1: RPC SUSY processes featuring gluino (a, b, c, d) or third generation squark (e, f) pair production studied in this analysis. RPV SUSY models considered are split in gluino pair production (g, h, i, j) and right-handed down squarks production in t-channel (k, l) which decay via baryon or lepton number violating couplings  $\lambda''$  and  $\lambda'$  respectively.

## 2 The ATLAS detector

The ATLAS experiment [23] is a multi-purpose particle detector with a forward-backward symmetric cylindrical geometry and nearly  $4\pi$  coverage in solid angle.<sup>4</sup> The interaction point is surrounded by an inner detector (ID), a calorimeter system, and a muon spectrometer (MS).

The ID provides precision tracking of charged particles for pseudorapidities  $|\eta| < 2.5$  and is surrounded by a superconducting solenoid providing a 2 T axial magnetic field. It consists of pixel and silicon-microstrip detectors inside a transition radiation tracker. One significant upgrade for the  $\sqrt{s} = 13$  TeV running period is the presence of the Insertable B-Layer [36], an additional pixel layer close to the interaction point, which provides high-resolution hits at small radius to improve the tracking performance.

<sup>4</sup> ATLAS uses a right-handed coordinate system with its origin at the nominal interaction point (IP) in the centre of the detector and the z-axis along the beam pipe. The x-axis points from the IP to the centre of the LHC ring, and the y-axis points upward. Cylindrical coordinates  $(r, \phi)$  are used in the transverse plane,  $\phi$  being the azimuthal angle around the beam pipe. The pseudorapidity is defined in terms of the polar angle  $\theta$  as  $\eta = -\ln \tan(\theta/2)$ . Rapidity is defined as  $y = 0.5 \ln [(E + p_z)/(E - p_z)]$  where  $E$  denotes the energy and  $p_z$  is the component of the momentum along the beam direction.

In the pseudorapidity region  $|\eta| < 2.5$ , high-granularity lead/liquid-argon electromagnetic sampling calorimeters are used. A steel/scintillator tile calorimeter measures hadron energies for  $|\eta| < 1.7$ . The endcap and forward regions, spanning  $1.5 < |\eta| < 4.9$ , are instrumented with liquid-argon calorimeters for both the electromagnetic and hadronic measurements.

The MS consists of three large superconducting toroids with eight coils each, a system of trigger and precision-tracking chambers, which provide triggering and tracking capabilities in the ranges  $|\eta| < 2.4$  and  $|\eta| < 2.7$ , respectively.

A two-level trigger system is used to select events [37]. The first-level trigger is implemented in hardware. This is followed by the software-based High-Level Trigger stage, which can run offline-like reconstruction and calibration software, reducing the event rate to about 1 kHz.

### 3 Dataset and simulated event samples

The data were collected by the ATLAS detector during 2015 with a peak instantaneous luminosity of  $L = 5.2 \times 10^{33} \text{ cm}^{-2}\text{s}^{-1}$ , and up to end of October 2016 with a peak instantaneous luminosity of  $L = 1.4 \times 10^{34} \text{ cm}^{-2}\text{s}^{-1}$ . The mean number of  $pp$  interactions per bunch crossing (pile-up) in the dataset is of  $\langle\mu\rangle = 13.7$  in 2015 and  $\langle\mu\rangle = 24.2$  in 2016. After the application of beam, detector and data quality requirements, the integrated luminosity considered in this analysis corresponds to  $36.0 \text{ fb}^{-1}$ . The preliminary uncertainty on the combined 2015+2016 integrated luminosity is 3.2%. It is derived, following a methodology similar to that detailed in Ref. [38], from a preliminary calibration of the luminosity scale using  $x$ - $y$  beam-separation scans performed in August 2015 and May 2016.

Monte Carlo (MC) simulated event samples are used to estimate the low cross-section SM background and to model the SUSY signals. The detector or reducible background mainly coming from  $t\bar{t}$  is estimated from the data and described in details in Section 5. The MC samples are processed through an ATLAS detector simulation [39] based on GEANT4 [40] or a fast simulation using a parameterisation of the calorimeter response and GEANT4 for the ID and MS [41]. They are reweighted to match the pile-up conditions observed in the data and are reconstructed in the same manner as the data. The generator, parton shower, cross-section normalisation, PDF set and underlying-event tune of these samples are given in Table 1. In most of the cases, the cross-sections are normalized at next-to-leading order (NLO).

The SUSY signals are defined by an effective Lagrangian describing the interactions of a small number of new particles. They assume one production process and one decay channel with a 100% branching fraction. These processes are generated from Leading Order (LO) matrix elements with up to two extra partons (only up to one for the  $\tilde{g} \rightarrow q\bar{q}(\ell\ell/\nu\nu)\tilde{\chi}_1^0$  model) using MG5\_AMC@NLO 2.2.3 [42] interfaced to Pythia 8.186 [43] with the A14 tune [50] for the modelling of the parton showering, hadronisation and underlying event. Jet-parton matching is realised following the CKKW-L prescription [54], with a matching scale set to one quarter of the pair-produced superpartner mass. The PDF set used for the generation is NNPDF23LO [49]. All signal models are generated with prompt decays of the SUSY particles. Signal cross-sections are generally calculated to NLO in the strong coupling constant, adding the resummation of soft gluon emission at next-to-leading-logarithmic accuracy (NLO+NLL) [44–48], except for RPV models of Fig.1(k) and Fig.1(l) as well as NUHM2 where NLO cross-sections are used [44, 55] cross-section is used. The nominal cross-section and the uncertainty are taken from an envelope of cross-section predictions using different PDF sets and factorisation and renormalisation scales, as described in Ref. [56]. Typical production cross-sections are:  $(86 \pm 15) \text{ fb}$  for gluino pairs with a mass of 1.2 TeV,

Physics process	Generator	Parton shower	Cross-section normalisation	PDF set	Tune
RPC signal	MG5_AMC@NLO 2.2.3 [42]	PYTHIA 8.186 [43]	NLO+NLL [44–48] or NLO-Prospino2	NNPDF2.3LO [49]	A14 [50]
RPV signal	MG5_AMC@NLO 2.2.3	PYTHIA 8.210	NLO+NLL or NLO-Prospino2	NNPDF2.3LO	A14
$t\bar{t} + W/Z/\gamma^*$ Diboson	MG5_AMC@NLO 2.2.2 SHERPA 2.1.1 [51]	PYTHIA 8.186 SHERPA 2.1.1	NLO [42] LO	NNPDF2.3LO CT10	A14 SHERPA default
$t\bar{t}H$	MG5_AMC@NLO 2.2.2	HERWIG 2.7.1 [52]	NLO [53]	CTEQ6L1	A14
$H + W/Z$	MG5_AMC@NLO 2.2.2	PYTHIA 8.186	NLO [53]	NNPDF2.3LO	A14
$t\bar{t} + WW/t\bar{t}$	MG5_AMC@NLO 2.2.2	PYTHIA 8.186	NLO [42]	NNPDF2.3LO	A14
$t + Z/WW/t\bar{t}$	MG5_AMC@NLO 2.2.2	PYTHIA 8.186	LO	NNPDF2.3LO	A14
Triboson	SHERPA 2.1.1	SHERPA 2.1.1	LO, NLO	CT10	SHERPA default

Table 1: Simulated signal and background event samples: the corresponding generator, parton shower, cross-section normalisation, PDF set and underlying-event tune are shown. Because of their very small contribution to the signal region background estimate  $t\bar{t}H$ ,  $t\bar{t} + WW/t\bar{t}$ ,  $t + Z/WW/t\bar{t}$ ,  $H + W/Z$  and triboson are summed and called 'Rare' in the following. NLO-Prospino2 refers to RPV down squark models of Fig.1(k) and (l), as well as NUHM2.

(518  $\pm$  67) fb for bottom squark pairs with a mass of 500 GeV, and (110  $\pm$  8) fb for right-handed down squark pairs with a mass of 500 GeV and a gluino mass of 1.5 TeV.

The two dominant background processes are  $t\bar{t}V$  (with  $V = W$  and  $Z$ , including non-resonant  $Z/\gamma^*$  contributions) and diboson with four charged leptons ( $\ell$ ), three charged leptons and one neutrino, or two charged leptons and two neutrinos. They are described in details in Ref. [57] and [58], respectively. In the matrix element, the former includes one ( $t\bar{t}Z$ ) and two ( $t\bar{t}W$ ) extra partons. Similarly for the latter, one ( $W^\pm W^\pm jj$ ) and two ( $WZ$ ,  $ZZ$ ) extra partons are simulated. NLO cross-sections for  $t\bar{t}W$ ,  $t\bar{t}Z$  with  $Z$  on-shell/off-shell and dibosons are respectively 600.8 fb, 839.3 fb [59]/123.7 fb, 40.0 pb [58].

Lower cross-section background processes are also considered and regrouped into 'Rare' in the following. This category contains samples of  $t\bar{t}WW$  with no extra parton in the matrix element,  $t\bar{t}H$ <sup>5</sup>,  $t\bar{t}t\bar{t}$ ,  $tZ$ ,  $t\bar{t}t$ ,  $tWZ$  as well as triboson ( $WWW$ ,  $WWZ$ ,  $WZZ$  and  $ZZZ$ ) with up to six charged leptons. The  $4\ell$  and  $2\ell + 2\nu$  processes are calculated at NLO for up to one additional parton; final states with two and three additional partons are calculated at leading order (LO). The  $WWZ \rightarrow 4\ell + 2\nu$  or  $2\ell + 4\nu$  processes are calculated at LO with up to two additional partons. The  $3\ell + 1\nu$  process is calculated at NLO and up to three extra partons at LO using the Comix [61] and OpenLoops [62] matrix element generators and merged with the SHERPA parton shower [63] using the ME+PS@NLO prescription [64]. The  $WWZ/WZZ \rightarrow 3\ell + 3\nu$ ,  $ZZZ \rightarrow 6\ell + 0\nu$ ,  $4\ell + 2\nu$  or  $2\ell + 4\nu$  processes are calculated with the same configuration but with up to only two extra partons at LO.

In all MC samples, except those produced by SHERPA, the EvtGEN v1.2.0 program [65] is used to model the properties of the bottom and charm hadron decays. To simulate the effects of additional  $pp$  collisions in the same and nearby bunch crossings, additional interactions are generated using the soft QCD processes of PYTHIA 8.186 with the A2 tune [66] and the MSTW2008LO PDF [67], and overlaid onto the simulated hard scatter event.

<sup>5</sup> The UEEE5 underlying-event tune is used together with the CTEQ6L1 [60] (matrix element) and CT10 (parton shower) PDF sets.



## 4 Event selection

Candidate events are required to have a reconstructed vertex [68], with at least two associated tracks with  $p_T > 400$  MeV, and the vertex with the highest sum of squared transverse momentum of the tracks is considered as the primary vertex. In order to perform background estimations using data, two categories of electrons and muons are defined: “candidate” and “signal” (the latter being a subset of the “candidate” leptons satisfying tighter selection criteria).

Electron candidates are reconstructed from energy depositions in the electromagnetic calorimeter that have been matched to an ID track and are required to have  $|\eta| < 2.47$ , a transverse momentum  $p_T > 10$  GeV, and to pass a loose likelihood-based identification requirement [69]. The likelihood input variables include measurements of calorimeter shower shapes and track properties from the ID. Candidates within the transition region between the barrel and endcap electromagnetic calorimeters,  $1.37 < |\eta| < 1.52$ , are removed. The track matched with the electron must have a significance of the transverse impact parameter with respect to the reconstructed primary vertex,  $d_0$ , of  $|d_0|/\sigma(d_0) < 5$ .

Muon candidates are reconstructed in the region  $|\eta| < 2.5$  from muon spectrometer tracks matching ID tracks. All muon candidates must have  $p_T > 10$  GeV and must pass the medium identification requirements [70], based on selections on the number of hits in the different ID and muon spectrometer subsystems, and the significance of the charge-to-momentum ratio  $q/p$  [70].

Jets are reconstructed with the anti- $k_t$  algorithm [71] with radius parameter  $R = 0.4$ , using three-dimensional topological energy clusters in the calorimeter [72] as input. All jets must have  $p_T > 20$  GeV and  $|\eta| < 2.8$ . Jets are calibrated as described in Ref. [73]. In order to reduce the effects of pile-up, for jets with  $p_T < 60$  GeV and  $|\eta| < 2.4$  a significant fraction of the tracks associated with each jet must have an origin compatible with the primary vertex, as defined by the jet vertex tagger [74]. Furthermore, for all jets the expected average energy contribution from pile-up clusters is subtracted according to the jet area [73].

Identification of jets containing  $b$ -hadrons ( $b$ -tagging) is performed with the MV2c10 algorithm, a multivariate discriminant making use of track impact parameters and reconstructed secondary vertices [75, 76]. A requirement is chosen corresponding to a 70% average efficiency for tagging  $b$ -jets in simulated  $t\bar{t}$  events. The rejection factors for light-quark/gluon jets,  $c$ -quark jets and hadronically decaying  $\tau$  leptons in simulated  $t\bar{t}$  events are approximately 380, 12 and 54, respectively [76, 77]. Jets with  $|\eta| < 2.5$  which satisfy this  $b$ -tagging requirement are identified as  $b$ -jets. To compensate for differences between data and MC simulation in the  $b$ -tagging efficiencies and mis-tagging rates, correction factors are applied to the simulated samples [76].

After object identification, overlaps between the different objects are resolved. Any jet within a distance  $\Delta R_y = \sqrt{(\Delta y)^2 + (\Delta \phi)^2} = 0.2$  of a lepton candidate is discarded, unless the jet has a value of the MV2c10 discriminant larger than the value corresponding to approximately 85%  $b$ -tagging efficiency, in which case the lepton is discarded since it is likely originating from a semileptonic  $b$ -hadron decay. Any remaining lepton within  $\Delta R_y = \min\{0.4, 0.1 + 9.6 \text{ GeV}/p_T(\ell)\}$  of a non-pileup jet is discarded. However, if the jet has fewer than three associated tracks or the muon  $p_T$  has more than  $0.5 p_T^{\text{jet}}$  and more than  $0.7 \sum p_T^{\text{jet tracks}}$ , where  $\sum p_T^{\text{jet tracks}}$  is the sum of track  $p_T$  for the tracks inside the jet, the muon is retained and the jet is discarded instead to avoid inefficiencies for high-energy muons undergoing significant energy loss in

the calorimeter. Any calo-tagged muon<sup>6</sup> sharing an ID track with an electron is removed. Finally, any electron sharing an ID track with the remaining muons is also removed.

Signal electrons must satisfy a medium likelihood-based identification requirement [69] and have  $|\eta| < 2$  to reduce the impact of electron charge mis-identification. Furthermore, electrons that are likely to be reconstructed with an incorrect charge assignment are further rejected using  $d_0$ , the distance of the cluster position in the middle layer and the extrapolated track and other related properties, combined into a single classifier using a boosted decision tree. The selection requirement is chosen such that it achieves a rejection of electrons with a wrong charge assignment by a factor of 5-10. The efficiency to select electrons with a correct charge is about 97% integrated over  $|\eta|$  and  $p_T$ . Signal muons must fulfil the requirement of  $|d_0|/\sigma(d_0) < 3$ . The track associated to the signal leptons must have a longitudinal impact parameter with respect to the reconstructed primary vertex,  $z_0$ , satisfying  $|z_0 \sin \theta| < 0.5$  mm. Isolation requirements are applied to both the signal electrons and muons. The scalar sum of the  $p_T$  of tracks within a variable-size cone around the lepton, excluding its own track, must be less than 6% of the lepton  $p_T$ . The track isolation cone radius for electrons (muons)  $\Delta R_\eta = \sqrt{(\Delta\eta)^2 + (\Delta\phi)^2}$  is given by the smaller of  $\Delta R_\eta = 10 \text{ GeV}/p_T$  and  $\Delta R_\eta = 0.2$  (0.3), that is, a cone of size 0.2 (0.3) at low  $p_T$  but narrower for high- $p_T$  leptons. In addition, in the case of electrons the energy of calorimeter energy clusters in a cone of  $\Delta R_\eta = 0.2$  around the electron (excluding the deposition from the electron itself) must be less than 6% of the electron  $p_T$ . Simulated events are corrected to account for minor differences in the lepton trigger, reconstruction, identification and isolation efficiencies between data and MC simulation.

The missing transverse momentum (and its magnitude  $E_T^{\text{miss}}$ ) is defined as the negative vector sum of the transverse momenta of all identified physics objects (electrons, photons [78], muons, jets) and an additional soft term. The soft term is constructed from all tracks that are not associated with any physics object, and that are associated with the primary vertex. In this way, the  $E_T^{\text{miss}}$  is adjusted for the best calibration of the jets and the other identified physics objects above, while maintaining pile-up independence in the soft term [79, 80].

Events are selected using a combination (logical OR) of dilepton and  $E_T^{\text{miss}}$  triggers, the latter being used only for events with  $E_T^{\text{miss}} > 250 \text{ GeV}$ . The trigger-level requirements on  $E_T^{\text{miss}}$  and the leading and subleading lepton  $p_T$  are looser than those applied offline to ensure that trigger efficiencies are constant in the relevant phase space. Events of interest are selected if they contain at least two signal leptons with  $p_T > 20 \text{ GeV}$  (apart for two SRs where the second lepton should be greater than 10 GeV, see Table 2). If the event contains exactly two signal leptons, they are required to have the same electric charge. Events are discarded if they contain any jet failing basic quality selection criteria that reject detector noise and non-collision backgrounds [81].

To maximise the sensitivity to signal models of Figure 1, nineteen overlapping signal regions are defined as shown in Table 2, with requirements on the number of signal leptons ( $N_{\text{leptons}}^{\text{signal}}$ ), the number of  $b$ -jets with  $p_T > 20 \text{ GeV}$  ( $N_{b\text{-jets}}$ ), the number of jets with different  $p_T$  thresholds (25, 40 or 50 GeV) regardless of their flavour ( $N_{\text{jets}}$ ),  $E_T^{\text{miss}}$ , the effective mass ( $m_{\text{eff}}$ ), defined as the scalar sum of the  $p_T$  of the signal leptons and jets (regardless of their flavour) in the event plus the  $E_T^{\text{miss}}$ , and the charge of the leptons in the event. The values of acceptance times efficiency of the SR selections for the SUSY signal models typically range between [UPDATE]% for models with a light  $\tilde{\chi}_1^0$  and [UPDATE]% for models with a heavy  $\tilde{\chi}_1^0$ .

<sup>6</sup> A calo-tagged muon is a muon identified solely by calorimeter based identification (so no signal in MS) and are relevant only at  $|\eta| < 0.1$ .

Signal region Name	$N_{\text{leptons}}^{\text{signal}}$	$N_{b\text{-jets}}$	$N_{\text{jets}}$	$p_{T,\text{jet}}$ [GeV]	$E_{\text{T}}^{\text{miss}}$ [GeV]	$m_{\text{eff}}$ [GeV]	$E_{\text{T}}^{\text{miss}}/m_{\text{eff}}$	Other	Targeted Signal
Rpc2L3bS	$\geq 2\text{SS}$	$\geq 3$	$\geq 6$	$> 25$	$> 150$	–	$> 0.2$	–	Fig. 1(a)
Rpc2L3bH	$\geq 2\text{SS}$	$\geq 3$	$\geq 6$	$> 25$	$> 250$	$> 1200$	–	–	Fig. 1(a), NUHM2
Rpc2Lsoft1b	$\geq 2\text{SS}$	$\geq 1$	$\geq 6$	$> 25$	$> 100$	–	$> 0.3$	$20, 10 < p_{\text{T}}^{\ell_1}, p_{\text{T}}^{\ell_2} < 100$ GeV	Fig. 1(b)
Rpc2Lsoft2b	$\geq 2\text{SS}$	$\geq 2$	$\geq 6$	$> 25$	$> 200$	$> 600$	$> 0.25$	$20, 10 < p_{\text{T}}^{\ell_1}, p_{\text{T}}^{\ell_2} < 100$ GeV	Fig. 1(b)
Rpc2L0bS	$\geq 2\text{SS}$	$= 0$	$\geq 6$	$> 25$	$> 150$	$> 600$	$> 0.25$	–	Fig. 1(c)
Rpc2L0bH	$\geq 2\text{SS}$	$= 0$	$\geq 6$	$> 40$	$> 250$	$> 900$	–	–	Fig. 1(c)
Rpc3L0bS	$\geq 3$	$= 0$	$\geq 4$	$> 40$	$> 200$	–	–	–	Fig. 1(d)
Rpc3L0bH	$\geq 3$	$= 0$	$\geq 4$	$> 40$	$> 200$	$> 1600$	–	–	Fig. 1(d)
Rpc3L1bS	$\geq 3$	$\geq 1$	$\geq 4$	$> 40$	$> 200$	$> 600$	–	–	Fig. 1(d) ??
Rpc3L1bH	$\geq 3$	$\geq 1$	$\geq 4$	$> 40$	$> 200$	$> 1600$	–	–	Fig. 1(d) ??
Rpc2L1bS	$\geq 2\text{SS}$	$\geq 1$	$\geq 6$	$> 25$	$> 150$	$> 600$	$> 0.25$	–	Fig. 1(e)
Rpc2L1bH	$\geq 2\text{SS}$	$\geq 1$	$\geq 6$	$> 25$	$> 250$	$> 1250$	$> 0.2$	–	Fig. 1(e)
Rpc3LSS1b	$\geq \ell^\pm \ell^\pm \ell^\pm$	$\geq 1$	–	–	–	–	–	veto $81 < m_{e^+e^+} < 101$ GeV	Fig. 1(f)
Rpv2L1bH	$\geq 2\text{SS}$	$\geq 1$	$\geq 6$	$> 50$	–	$> 2000$	–	–	Figs. 1(g), 1(h)
Rpv2L0b	$= 2\text{SS}$	$= 0$	$\geq 6$	$> 40$	–	$> 1800$	–	veto $81 < m_{e^+e^+} < 101$ GeV	Fig. 1(i)
Rpv2L3bH	$\geq 2\text{SS}$	$\geq 3$	$\geq 6$	$> 40$	–	$> 1800$	–	veto $81 < m_{e^+e^+} < 101$ GeV	Fig. 1(j)
Rpv2L3bS	$\geq \ell^- \ell^-$	$\geq 3$	$\geq 3$	$> 50$	–	$> 1200$	–	–	Fig. 1(k)
Rpv2L1bS	$\geq \ell^- \ell^-$	$\geq 1$	$\geq 4$	$> 50$	–	$> 1200$	–	–	Fig. 1(l)
Rpv2L1bM	$\geq \ell^- \ell^-$	$\geq 1$	$\geq 4$	$> 50$	–	$> 1800$	–	–	Fig. 1(l)

Table 2: Summary of the signal region definition. Unless explicitly stated in the table, at least two signal leptons with  $p_{\text{T}} > 20$  GeV and same charge (SS) are required in each signal region. Requirements are placed on the number of signal leptons ( $N_{\text{lept}}^{\text{signal}}$ ), the number of jets ( $N_{\text{jets}}$ ) or the number of  $b$ -jets with  $p_{\text{T}} > 20$  GeV ( $N_{b\text{-jets}}$ ),  $p_{\text{T}}$  of the lepton or jet,  $E_{\text{T}}^{\text{miss}}$ ,  $m_{\text{eff}}$  or  $E_{\text{T}}^{\text{miss}}/m_{\text{eff}}$ . The last column indicates the targeted signal model.

## 5 Background estimation

Two main sources of SM background can be distinguished in this analysis. The first category is the reducible or detector background which includes events containing electrons with mis-measured charge, mainly from the production of top quark pairs, and events containing at least one non-prompt or fake lepton, which mainly originate from hadron decays in events containing top quarks or  $W$  bosons produced in association with jets. Data-driven methods used for the estimation of this background are described in Section 5.1. The second category consists of events with two same-sign prompt leptons or at least three prompt leptons and estimated with the MC samples described in Section 3. Since diboson and  $t\bar{t}V$  events are the main backgrounds in the signal regions, dedicated validation regions with an enhanced contribution from these processes are defined to verify the background predictions (see Section 5.2).

### 5.1 Detector background estimation methods

Background events due to charge mis-identification, dominated by electrons having emitted a hard bremsstrahlung photon which subsequently converted to an electron–positron pair, are referred to as “charge-flip”. The probability of mis-identifying the charge of a muon is checked in both data and MC simulation, and found to be negligible in the kinematic range relevant to this analysis. The contribution of charge-flip events is estimated using the data. The electron charge-flip probability is extracted in a  $Z/\gamma^* \rightarrow ee$  data sample using a likelihood fit which takes as input the numbers of same-sign and opposite-sign electron pairs observed in a window around the  $Z$  mass. The charge-flip probability is a free parameter of the fit and is extracted as a function of the electron  $p_{\text{T}}$  and  $\eta$ . These probabilities are in the range **UPDATE: 1–5%**

and **UPDATE:0.1–1%** for the loose and baseline electron respectively. The event yield of this background in the signal or validation regions is obtained by applying the measured charge-flip probability to data regions with the same kinematic requirements as the signal or validation regions but with opposite-sign lepton pairs.

The contribution from fake or non-prompt (FNP) leptons (such as hadrons mis-identified as leptons, leptons originating from heavy-flavour decays, and electrons from photon conversions) is also estimated from the data with a matrix method similar to that described in Ref. [82]. In this method, two types of lepton identification criteria are defined: “tight”, corresponding to the signal lepton criteria described in Section 4, and “loose”, corresponding to candidate leptons after overlap removal. The matrix method relates the number of events containing prompt or FNP leptons to the number of observed events with tight or loose-not-tight leptons using the probability for loose prompt or FNP leptons to satisfy the tight criteria. The probability for loose prompt leptons to satisfy the tight selection criteria ( $\epsilon$ ) is obtained using a  $Z/\gamma^* \rightarrow \ell\ell$  data sample and is modelled as a function of the lepton  $p_T$  and  $\eta$ . The probability for loose FNP leptons to satisfy the tight selection criteria (FNP fake rate,  $f$ ) is determined from data in a SS control region enriched in non-prompt leptons originating from heavy-flavour decays, mostly coming from semileptonic  $t\bar{t}$  events. This region contains events with at least one  $b$ -jet, one well-isolated “tag” muon, and an additional loose electron or muon on which the measurement is performed. The efficiencies are measured as function of  $p_T$  after subtracting the small contribution from prompt lepton processes.

The estimated FNP yields in the SRs are consistent with those predicted by two alternative methods: the first one relies on MC simulation of processes with FNP leptons or charge-flipped electrons ( $t\bar{t}$ ,  $V$ +jets) [22, 83], corrected to match the observed data in dedicated control regions. The second method relies on data events with only one lepton, which are the processes leading to FNP leptons, to extrapolate from low- $E_T^{\text{miss}}$  control regions to the SRs. **[UPDATE: inflate this section]**

## 5.2 Validation of background estimates

To check the validity and robustness of the background estimates, the distributions of several discriminating variables in data are compared with the predicted background after various requirements on the number of jets and  $b$ -jets. Examples of such distributions are shown in Fig. 2, and illustrate that the predictions and data agree fairly well.

Dedicated validation regions (VRs) are defined to test the estimate of the  $t\bar{t}V$ ,  $WZ$  and  $W^\pm W^\pm$  SM processes contributing to the signal regions. The corresponding selections are summarized in Table 3. In these regions, the overlap with the signal regions is resolved by vetoing events that contribute to the signal regions. To further reduce contributions from electron charge mis-identification, events are also vetoed in VR- $t\bar{t}W$  and VR- $W^\pm W^\pm jj$  if one of the two leading leptons is an electron with  $|\eta| > 1.37$  **[UPDATE:Still true]**, since contributions from charge-flip electrons are smaller in the central region due to the lower amount of detector material in front of the calorimeters. The purity of the targeted processes in these regions ranges from about **[UPDATE:20% to 50%]**.

The observed yields in these validation regions, compared with the background predictions and uncertainties, can be seen in Table 4. There is good agreement between data and the estimated background for the validation regions.

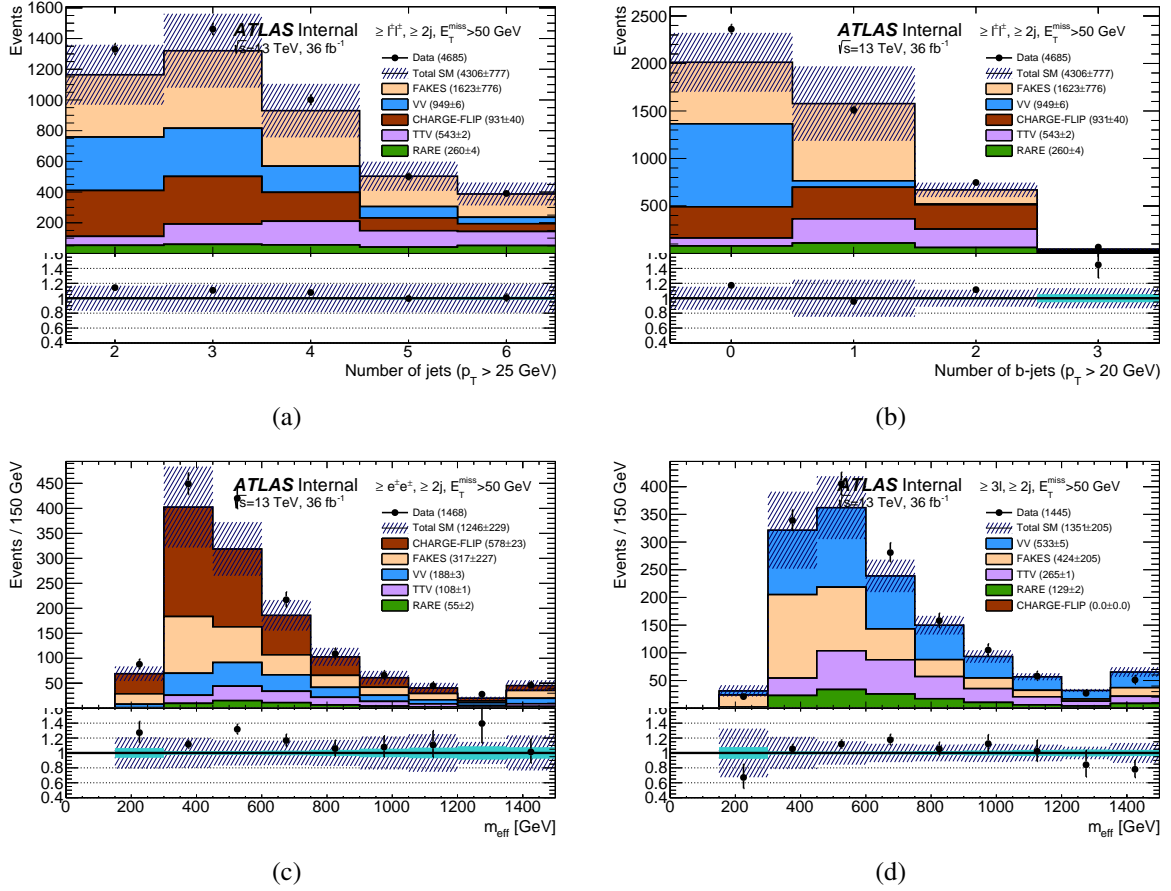


Figure 2: Distributions of the number of jets (a), of  $b$ -tagged jets (b) and the effective mass (c,d) after requiring at least two jets ( $p_T > 25$  GeV) and  $E_T^{\text{miss}} > 50$  GeV, as well as at least two same-sign leptons (a,b) or two same-sign electrons (c) or three leptons (d).  $m_{\text{eff}}$  distributions in the validation regions are shown in (e) and (f). The statistical uncertainties in the background prediction are included in the uncertainty band, as well as the full systematic uncertainties for backgrounds with fake or non-prompt leptons, or charge-flip. The light-shaded bands in the ratio plots show contributions from statistical uncertainties alone. The “Rare” category contains the contributions from associated production of  $t\bar{t}$  with  $h$ / $WW$ / $t\bar{t}$ , as well as  $tZ$ ,  $tWZ$ ,  $Wh$ ,  $Zh$ , and triboson production. [UPDATE: Remove numbers in the legend and move from upper case to lower case.]

## 6 Systematic uncertainties on the background estimation

Figure 3 summarises the contributions of the different sources of systematic uncertainty in the total SM background predictions in the signal regions.

The systematic uncertainties related to the same-sign prompt leptons background estimation arise from the accuracy of the theoretical and experimental modelling in the MC simulation. The primary sources of systematic uncertainties are related to the jet energy scale calibration, jet energy resolution,  $b$ -tagging efficiency, and MC modelling and theoretical cross-section uncertainties. The statistical uncertainty of the simulated event samples is also taken into account.

The cross-sections used to normalise the MC samples are varied according to the uncertainty in the cross-section calculation, that is, 13% for  $t\bar{t}W$  and 12%  $t\bar{t}Z$  production [59], and 6% for diboson production.

Validation Region Name	$N_{\text{lept}}^{\text{signal}} (N_{\text{lept}}^{\text{cand}})$	$N_{b\text{-jets}}$	$N_{\text{jets}}$	$p_{T,\text{jet}}$ [GeV]	$E_{\text{T}}^{\text{miss}}$ [GeV]	$m_{\text{eff}}$ [GeV]	Other
$W^\pm W^\pm jj$	= 2 (= 2) = 1 SS pair	= 0	$\geq 2$	> 50	> 55	> 650	veto $81 < m_{e^\pm e^\pm} < 101$ GeV $p_{\text{T}}^{\ell_2} > 30$ GeV $\min\{\Delta R(\ell_{1,2}, j)\} > 0.7$ $\min\{\Delta R(\ell_1, \ell_2)\} > 1.3$
$WZ4j$	= 3 (= 3)	= 0	$\geq 4$	> 25	–	> 450	$E_{\text{T}}^{\text{miss}} / \sum p_{\text{T}}^\ell < 0.7$
$WZ5j$	= 3 (= 3)	= 0	$\geq 5$	> 25	–	> 450	$E_{\text{T}}^{\text{miss}} / \sum p_{\text{T}}^\ell < 0.7$
$t\bar{t}W$	= 2 (= 2) = 1 SS pair	$\geq 1$	$\geq 4 (e^\pm e^\pm, e^\pm \mu^\pm)$ $\geq 3 (\mu^\pm \mu^\pm)$	> 40 > 25	> 45	> 550	$p_{\text{T}}(\ell_2) > 40$ GeV $\sum p_{\text{T}}^{b\text{-jet}} / \sum p_{\text{T}}^{jet} > 0.25$
$t\bar{t}Z$	$\geq 3$ (-) $\geq 1$ SFOS pair	$\geq 1$	$\geq 3$	> 35	–	> 450	$81 < m_{\text{SFOS}} < 101$ GeV
All VRs	Veto events belonging to any SR, except Rpc3LSS1b. For Rpv2L3bS, Rpv2L1bS, Rpv2L1bM, veto also positively-charged lepton pairs and for Rpv2L0b and Rpv2L3bH remove the $m_{e^\pm e^\pm}$ veto.						

Table 3: Summary of the event selection in the validation regions (VRs). Requirements are placed on the number of signal leptons ( $N_{\text{lept}}^{\text{signal}}$ ) and candidate leptons ( $N_{\text{lept}}^{\text{cand}}$ ), the number of jets ( $N_{\text{jets}}$ ) or the number of  $b$ -jets with  $p_{\text{T}} > 20$  GeV ( $N_{b\text{-jets}}$ ),  $p_{\text{T}}$  of the lepton or jet,  $E_{\text{T}}^{\text{miss}}$  and  $m_{\text{eff}}$ . The three leading- $p_{\text{T}}$  leptons are referred to as  $\ell_{1,2,3}$  with decreasing  $p_{\text{T}}$ . In some validation regions, additional requirements are set on electron pseudorapidity, on the invariant mass of the two leading electrons  $m_{ee}$ , the presence of SS leptons or a pair of same-flavour opposite-sign leptons (SFOS) and its invariant mass  $m_{\text{SFOS}}$  or the distance between the leptons and the jets or the two leptons.

Validation Region	$WZ4j$	$WZ5j$	$W^\pm W^\pm jj$	$t\bar{t}W$	$t\bar{t}Z$
$t\bar{t}Z/\gamma^*$	$\pm$	$\pm$	$\pm$	$\pm$	$\pm$
$t\bar{t}W$	$\pm$	$\pm$	$\pm$	$\pm$	$\pm$
DiBosons	$\pm$	$\pm$	$\pm$	$\pm$	$\pm$
Rare	$\pm$	$\pm$	$\pm$	$\pm$	$\pm$
Fake/non-prompt leptons	$\pm$	$\pm$	$\pm$	$\pm$	$\pm$
Charge-flip	–	$\pm$	$\pm$	$\pm$	–
Total SM background	–	$\pm$	$\pm$	$\pm$	–
Observed	–	$\pm$	$\pm$	$\pm$	–

Table 4: The numbers of observed data and expected background events for the validation regions. The “Rare” category contains the contributions from associated production of  $t\bar{t}$  with  $h/WW/t/t\bar{t}$ , as well as  $tZ$ ,  $tWZ$ ,  $Wh$ ,  $Zh$ , and triboson production. Background categories shown as “–” denote that they cannot contribute to a given region (e.g. charge flips in 3-lepton regions). The displayed yields include all sources of statistical and systematic uncertainties, except for the theoretical uncertainties which only consist of uncertainties on the inclusive production cross-sections.

Additional uncertainties are assigned to these backgrounds to account for the modelling of the kinematic distributions in the MC simulation. For  $t\bar{t}W$  and  $t\bar{t}Z$ , the predictions from the MG5\_AMC@NLO and SHERPA generators are compared, and the renormalisation and factorisation scales used to generate these samples are varied, leading to a  $\sim$ [UPDATE:30%] uncertainty for these processes after the SR selections. For dibosons, uncertainties are estimated by varying the renormalisation, factorisation and resummation scales, leading to a  $\sim$ [UPDATE:40-50%] uncertainty for these processes after the SR selections. For triboson,  $t\bar{t}H$ ,  $t\bar{t}t\bar{t}$  and  $tZ$  production processes, which constitute small backgrounds in most of the signal regions, a [UPDATE:50%] uncertainty on their total contribution is assumed.



Uncertainties in the FNP lepton background estimate are assigned due to the limited number of data events with loose and tight leptons. In addition, systematic uncertainties of [UPDATE:50-60%] are assigned to the FNP fake rate for potentially different compositions (heavy flavour, light flavour or conversions) between the regions used to measure these probabilities and the SRs, as well as the contamination from prompt leptons in the former regions. Similarly [UPDATE:5%] systematic is assigned to  $\epsilon$  determination. This leads to overall FNP background uncertainties in the total background estimates of [UPDATE:5–32%] depending on the signal region.

The error on the electron charge-flip probability mainly originates from the limited statistics used in the charge-flip probability measurement regions and the background contamination beyond the  $Z$  peak. The relative error on the charge-flip is below [UPDATE:20%] for  $p_T$  above 20 GeV.

## 7 Results, interpretation and limits

Figure 4 shows the  $E_T^{\text{miss}}$  or  $m_{\text{eff}}$  distributions after the signal region selections (except that on the variable shown). The expected contributions from the SM backgrounds are also shown.

The detailed yields for data and the different sources of SM background in the signal regions are presented in Table 5. None of the observed events in data contain three leptons of equal charge. The uncertainties amount to [UPDATE:25–50%] of the total background depending on the signal region. The contributions listed in the “Rare” category in the tables is dominated by  $tWZ$  and triboson production in SRs with 3 leptons, by  $t\bar{t}H$  and  $tWZ$  production in SRs with a  $b$ -jet veto, by  $t\bar{t}H$  and  $t\bar{t}t\bar{t}$  production in SRs requiring one  $b$ -jet and by  $t\bar{t}t\bar{t}$  production in SRs with three  $b$ -jets required.

In the absence of any significant deviations from the SM predictions, upper limits on possible BSM contributions to the signal regions are computed, using the SUSY benchmark scenarios described in Section 1. The HistFitter framework [84], which utilises a profile-likelihood-ratio test [85], is used to establish 95% confidence intervals using the  $\text{CL}_s$  prescription [86]. The likelihood is built as the product of a Poisson probability density function describing the observed number of events in the signal region and Gaussian distributions constraining the nuisance parameters associated with the systematic uncertainties whose widths correspond to the sizes of these uncertainties; Poisson distributions are used instead for MC and data control region statistical uncertainties.

Correlations of a given nuisance parameter between the different sources of backgrounds and the signal are taken into account when relevant. The hypothesis tests are performed independently for each of the signal regions.

Table 5 presents 95% confidence level (CL) model-independent upper limits on the number of observed (expected) BSM events,  $S_{\text{obs}}^{95}$  ( $S_{\text{exp}}^{95}$ ), that may contribute to the signal regions. Normalising these by the integrated luminosity  $L$  of the data sample, they can be interpreted as upper limits on the visible BSM cross-section, defined as the product  $\sigma_{\text{prod}} \times A \times \epsilon = S_{\text{obs}}^{95}/L$  of production cross-section ( $\sigma_{\text{prod}}$ ), acceptance ( $A$ ) and reconstruction efficiency ( $\epsilon$ ).

Exclusion limits are also set on the masses of the superpartners involved in the SUSY benchmark scenarios considered in this analysis. Simplified models corresponding to a single production mode and with 100% branching ratio to a specific decay chain are used, with the masses of the SUSY particles not involved in the process set to very high values. Figure 5, 6 and 7 show the limits on all the models considered in Figure 1. UPDATE: comment theplots when available

Signal Region	Rpc2L3bS	Rpc2L3bH	Rpc2Lsoft1b	Rpc2Lsoft2b	Rpc2L0bS	Rpc2L0bH
$t\bar{t}Z\gamma^*$						
$t\bar{t}W$						
Diboson						
Rare						
Fake/non-prompt leptons						
Charge-flip						
Total Fitted bkg						
Observed						
$S_{\text{obs}}^{95}$ $S_{\text{exp}}^{95}$ $\langle A \times \epsilon \sigma_{\text{prod}} \rangle_{\text{obs}}^{95}$ [fb] $p_0$ (Z)						

Signal Region	Rpc3L0bS	Rpc3L0bH	Rpc3L1bS	Rpc3L1bH	Rpc2L1bS	Rpc2L1bH	Rpc3LSS1b
$t\bar{t}Z\gamma^*$							
$t\bar{t}W$							
Diboson							
Rare							
Fake/non-prompt leptons							
Charge-flip							
Total Fitted bkg							
Observed							
$S_{\text{obs}}^{95}$ $S_{\text{exp}}^{95}$ $\langle A \times \epsilon \sigma_{\text{prod}} \rangle_{\text{obs}}^{95}$ [fb] $p_0$ (Z)							

Signal Region	Rpv2L1bH	Rpv2L0b	Rpv2L3bH	Rpv2L3bS	Rpv2L1bS	Rpv2L1bM
$t\bar{t}Z\gamma^*$						
$t\bar{t}W$						
Diboson						
Rare						
Fake/non-prompt leptons						
Charge-flip						
Total Fitted bkg						
Observed						
$S_{\text{obs}}^{95}$ $S_{\text{exp}}^{95}$ $\langle A \times \epsilon \sigma_{\text{prod}} \rangle_{\text{obs}}^{95}$ [fb] $p_0$ (Z)						

Table 5: Numbers of events observed in the signal regions compared with background expectations obtained from the fits described in the text. Empty cells (indicated by a '-') correspond to estimates lower than 0.01. The p-values ( $p_0$ ) give the probabilities of the observations being consistent with the estimated backgrounds. For an observed number of events lower than expected, the p-value is truncated at 0.5. Between parentheses,  $p$ -values are also given as the number of equivalent Gaussian standard deviations (Z). Also shown are 95% CL upper limits on the visible cross-section ( $\langle \epsilon \sigma \rangle_{\text{obs}}^{95}$ ), the visible number of signal events ( $S_{\text{obs}}^{95}$ ) and the number of signal events ( $S_{\text{exp}}^{95}$ ) given the expected number of background events (and  $\pm 1\sigma$  excursions of the expectation). **[UPDATE:Put final numbers]**



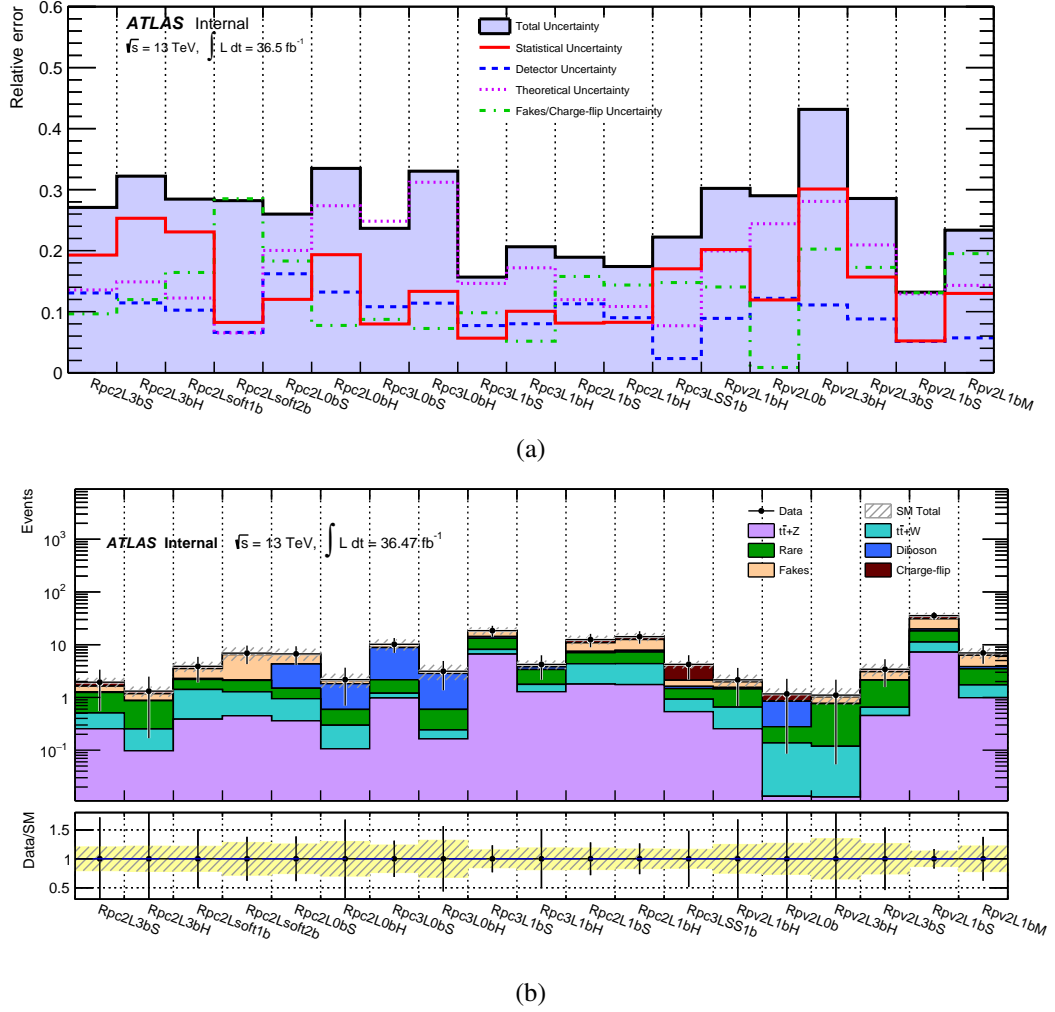


Figure 3: Relative systematic errors and comparison of the observed and expected event yields in each signal regions. The background expectations are those obtained from the background-only fits, presented in Table 5. **[UPDATE: Put all signal regions with final notations. Add ratio plot below SR Event Yields]**



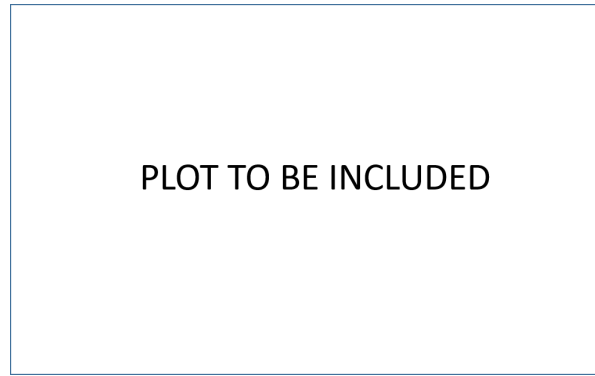
Figure 4: Missing transverse momentum distributions after (a) **UPDATE**, (b) **UPDATE**, (c) **UPDATE**, (d) **UPDATE**, (e) **UPDATE** and (f) **UPDATE** selection, except the  $E_T^{\text{miss}}$  requirement. The results in the signal regions are shown in the last (inclusive) bin of each plot. The statistical uncertainties in the background prediction are included in the uncertainty band, as well as the full systematic uncertainties for backgrounds with fake or non-prompt leptons, or charge-flip. **[UPDATE: Choose the illustrative SR plots (3 RPC, 3 RPV) and put the other in back-up]**



Figure 5: Observed and expected exclusion limits on the  $\tilde{g}$ ,  $\tilde{b}_1$ ,  $\tilde{t}_1$  and  $\tilde{\chi}_1^0$  masses in the context of RPC SUSY scenarios with simplified mass spectra. The signal region used to obtain the limits is specified for each scenario. The contours of the band around the expected limit are the  $\pm 1\sigma$  results, including all uncertainties except theoretical uncertainties on the signal cross-section. The dotted lines around the observed limit illustrate the change in the observed limit as the nominal signal cross-section is scaled up and down by the theoretical uncertainty. All limits are computed at 95% CL. The diagonal lines indicate the kinematic limit for the decays in each specified scenario. Results are compared with the observed limits obtained by previous ATLAS searches [22, 87–89]. [UPDATE: plots and captions].



Figure 6: Observed and expected exclusion limits on the  $\tilde{g}$ ,  $\tilde{t}_1$  and  $\tilde{d}_R$  masses in the context of RPV SUSY scenarios with simplified mass spectra featuring  $\tilde{g}\tilde{g}$  or  $\tilde{d}_R\tilde{d}_R$  pair production with exclusive decay modes. The signal region used to obtain the limits is specified for each scenario. The contours of the band around the expected limit are the  $\pm 1\sigma$  results, including all uncertainties except theoretical uncertainties on the signal cross-section. The dotted lines around the observed limit illustrate the change in the observed limit as the nominal signal cross-section is scaled up and down by the theoretical uncertainty. All limits are computed at 95% CL. The diagonal lines indicate the kinematic limit for the decays in each specified scenario, or in the case of  $\tilde{d}_R\tilde{d}_R$  production, the region where the alternative decay channel  $\tilde{d}_R \rightarrow \tilde{g}d$  is open. Results are compared with the observed limits obtained by previous ATLAS searches [89]. [UPDATE: plots and captions].



(a)

Figure 7: Observed and expected exclusion limits in the  $m_{1/2}$  versus  $m_H^2$  plane for the NUHM2 model described in the text. The contours of the band around the expected limit are the  $\pm 1\sigma$  results, including all uncertainties except theoretical uncertainties on the signal cross-section. The dotted lines around the observed limit illustrate the change in the observed limit as the nominal signal cross-section is scaled up and down by the theoretical uncertainty. All limits are computed at 95% CL. **[UPDATE: plots and Caption]**.

## 8 Conclusion

A search for supersymmetry in events with exactly two same-sign leptons or at least three leptons, multiple jets,  $b$ -jets and large  $E_{\text{T}}^{\text{miss}}$  and/or  $m_{\text{eff}}$  is presented. The analysis is performed with proton–proton collision data at  $\sqrt{s} = 13$  TeV collected between August 2015 and October 2016 with the ATLAS detector at the Large Hadron Collider corresponding to an integrated luminosity of  $36.0 \text{ fb}^{-1}$ . With no significant excess over the Standard Model expectation observed, results are interpreted in the framework of simplified models featuring gluino and squark production in  $R$ -parity conserving and  $R$ -parity violating scenarios. In the  $\tilde{g}\tilde{g}$  simplified models considered,  $m_{\tilde{g}} \lesssim [\text{UPDATE}] \text{ TeV}$  and  $m_{\tilde{\chi}_1^0} \lesssim [\text{UPDATE}] \text{ TeV}$  are excluded at 95% confidence level depending on the model parameters. Bottom squark masses of  $m_{\tilde{b}_1} \lesssim [\text{UPDATE}] \text{ GeV}$  are also excluded for a light  $\tilde{\chi}_1^0$  in a  $\tilde{b}_1\tilde{b}_1^*$  simplified model with  $\tilde{b}_1 \rightarrow tW^-\tilde{\chi}_1^0$ . Right-handed down squark masses are probed up to  $m_{\tilde{d}_R} \approx [\text{UPDATE}] \text{ GeV}$  in RPV scenarios. Within the models considered, exclusion limits are extended by  $[\text{UPDATE}] \text{ GeV}$  in  $\tilde{g}$  mass,  $[\text{UPDATE}] \text{ GeV}$  in  $\tilde{\chi}_1^0$  mass and  $[\text{UPDATE}] \text{ GeV}$  in  $\tilde{b}_1$  mass with respect to previous results.

## References

- [1] Yu. A. Golfand and E. P. Likhtman, *Extension of the Algebra of Poincare Group Generators and Violation of P Invariance*, JETP Lett. **13** (1971) 323, [Pisma Zh. Eksp. Teor. Fiz.13,452(1971)].
- [2] D. V. Volkov and V. P. Akulov, *Is the Neutrino a Goldstone Particle?*, Phys. Lett. **B46** (1973) 109.
- [3] J. Wess and B. Zumino, *Supergauge Transformations in Four-Dimensions*, Nucl. Phys. **B70** (1974) 39.
- [4] J. Wess and B. Zumino, *Supergauge Invariant Extension of Quantum Electrodynamics*, Nucl. Phys. **B78** (1974) 1.
- [5] S. Ferrara and B. Zumino, *Supergauge Invariant Yang-Mills Theories*, Nucl. Phys. **B79** (1974) 413.
- [6] A. Salam and J. A. Strathdee, *Supersymmetry and Nonabelian Gauges*, Phys. Lett. **B51** (1974) 353.
- [7] S. P. Martin, *A Supersymmetry primer*, (1997), [Adv. Ser. Direct. High Energy Phys.18,1(1998)], arXiv: [hep-ph/9709356](https://arxiv.org/abs/hep-ph/9709356).
- [8] P. Fayet, *Supersymmetry and Weak, Electromagnetic and Strong Interactions*, Phys. Lett. **B64** (1976) 159.
- [9] P. Fayet, *Spontaneously Broken Supersymmetric Theories of Weak, Electromagnetic and Strong Interactions*, Phys. Lett. **B69** (1977) 489.
- [10] G. R. Farrar and P. Fayet, *Phenomenology of the Production, Decay, and Detection of New Hadronic States Associated with Supersymmetry*, Phys. Lett. **B76** (1978) 575.
- [11] H. Goldberg, *Constraint on the Photino Mass from Cosmology*, Phys. Rev. Lett. **50** (1983) 1419, [Erratum: Phys. Rev. Lett. **103** (2009) 099905].
- [12] J. R. Ellis et al., *Supersymmetric Relics from the Big Bang*, Nucl. Phys. **B238** (1984) 453.
- [13] N. Sakai, *Naturalness in Supersymmetric Guts*, Z. Phys. **C11** (1981) 153.

- [14] S. Dimopoulos, S. Raby and F. Wilczek, *Supersymmetry and the Scale of Unification*, *Phys. Rev.* **D24** (1981) 1681.
- [15] L. E. Ibanez and G. G. Ross, *Low-Energy Predictions in Supersymmetric Grand Unified Theories*, *Phys. Lett.* **B105** (1981) 439.
- [16] S. Dimopoulos and H. Georgi, *Softly Broken Supersymmetry and SU(5)*, *Nucl. Phys.* **B193** (1981) 150.
- [17] R. Barbieri and G. F. Giudice, *Upper Bounds on Supersymmetric Particle Masses*, *Nucl. Phys.* **B306** (1988) 63.
- [18] B. de Carlos and J. A. Casas, *One loop analysis of the electroweak breaking in supersymmetric models and the fine tuning problem*, *Phys. Lett.* **B309** (1993) 320, arXiv: [hep-ph/9303291](#).
- [19] K. Inoue et al., *Aspects of Grand Unified Models with Softly Broken Supersymmetry*, *Prog. Theor. Phys.* **68** (1982) 927, [Erratum: *Prog. Theor. Phys.* **70** (1983) 330].
- [20] J. R. Ellis and S. Rudaz, *Search for Supersymmetry in Toponium Decays*, *Phys. Lett.* **B128** (1983) 248.
- [21] C. Borschensky et al., *Squark and gluino production cross sections in pp collisions at  $\sqrt{s} = 13, 14, 33$  and 100 TeV*, *Eur.Phys.J.* **C74** (2014) 3174, arXiv: [1407.5066 \[hep-ph\]](#).
- [22] ATLAS Collaboration, *Search for supersymmetry at  $\sqrt{s} = 13$  TeV in final states with jets and two same-sign leptons or three leptons with the ATLAS detector*, *Eur. Phys. J.* **C76** (2016) 259, arXiv: [1602.09058 \[hep-ex\]](#).
- [23] ATLAS Collaboration, *The ATLAS Experiment at the CERN Large Hadron Collider*, *JINST* **3** (2008) S08003.
- [24] CMS Collaboration, *Search for new physics in same-sign dilepton events in proton-proton collisions at  $\sqrt{s} = 13$  TeV*, (2016), arXiv: [1605.03171 \[hep-ex\]](#).
- [25] J. Alwall et al., *Searching for Directly Decaying Gluinos at the Tevatron*, *Phys. Lett.* **B666** (2008) 34, arXiv: [0803.0019 \[hep-ph\]](#).
- [26] J. Alwall, P. Schuster and N. Toro, *Simplified Models for a First Characterization of New Physics at the LHC*, *Phys. Rev.* **D79** (2009) 075020, arXiv: [0810.3921 \[hep-ph\]](#).
- [27] D. Alves, *Simplified Models for LHC New Physics Searches*, *J. Phys.* **G39** (2012) 105005, ed. by N. Arkani-Hamed et al., arXiv: [1105.2838 \[hep-ph\]](#).
- [28] P. Huang et al., *Same-Sign Dilepton Excesses and Light Top Squarks*, *Phys. Rev.* **D92** (2015) 075035, arXiv: [1507.01601 \[hep-ph\]](#).
- [29] J. R. Ellis et al., *Exploration of the MSSM with nonuniversal Higgs masses*, *Nucl. Phys.* **B652** (2003) 259, arXiv: [hep-ph/0210205 \[hep-ph\]](#).
- [30] J. R. Ellis, K. A. Olive and Y. Santoso, *The MSSM parameter space with nonuniversal Higgs masses*, *Phys. Lett.* **B539** (2002) 107, arXiv: [hep-ph/0204192 \[hep-ph\]](#).
- [31] E. Nikolidakis and C. Smith, *Minimal Flavor Violation, Seesaw, and R-parity*, *Phys.Rev.* **D77** (2008) 015021, arXiv: [0710.3129 \[hep-ph\]](#).

- [32] C. Smith, *Minimal Flavor Violation as an alternative to R-parity*, (2008), arXiv: [0809.3152 \[hep-ph\]](#).
- [33] C. Csaki, Y. Grossman and B. Heidenreich, *MFV SUSY: A Natural Theory for R-Parity Violation*, *Phys.Rev.* **D85** (2012) 095009, arXiv: [1111.1239 \[hep-ph\]](#).
- [34] G. Durieux and C. Smith, *The same-sign top signature of R-parity violation*, *JHEP* **10** (2013) 068, arXiv: [1307.1355 \[hep-ph\]](#).
- [35] J. Berger et al., *The Same-Sign Dilepton Signature of RPV/MFV SUSY*, *JHEP* **04** (2013) 077, arXiv: [1302.2146 \[hep-ph\]](#).
- [36] ATLAS Collaboration, *ATLAS Insertable B-Layer Technical Design Report*, CERN-LHCC-2010-013. ATLAS-TDR-19, 2010, URL: <http://cds.cern.ch/record/1291633>.
- [37] M. Aaboud et al., *Performance of the ATLAS Trigger System in 2015*, (2016), arXiv: [1611.09661 \[hep-ex\]](#).
- [38] ATLAS Collaboration, *Luminosity determination in pp collisions at  $\sqrt{s} = 8$  TeV using the ATLAS detector at the LHC*, *Eur. Phys. J.* **C76** (2016) 653, arXiv: [1608.03953 \[hep-ex\]](#).
- [39] ATLAS Collaboration, *The ATLAS Simulation Infrastructure*, *Eur.Phys.J.* **C70** (2010) 823, arXiv: [1005.4568 \[physics.ins-det\]](#).
- [40] S. Agostinelli et al., *GEANT4: A Simulation toolkit*, *Nucl.Instrum.Meth.* **A506** (2003) 250.
- [41] ATLAS Collaboration, *The simulation principle and performance of the ATLAS fast calorimeter simulation FastCaloSim*, ATL-PHYS-PUB-2010-013, 2010, URL: <https://cds.cern.ch/record/1300517>.
- [42] J. Alwall et al., *The automated computation of tree-level and next-to-leading order differential cross sections, and their matching to parton shower simulations*, *JHEP* **07** (2014) 079, arXiv: [1405.0301 \[hep-ph\]](#).
- [43] T. Sjöstrand, S. Mrenna and P. Z. Skands, *A Brief Introduction to PYTHIA 8.1*, *Comput. Phys. Commun.* **178** (2008) 852, arXiv: [0710.3820 \[hep-ph\]](#).
- [44] W. Beenakker et al., *Squark and gluino production at hadron colliders*, *Nucl.Phys.* **B492** (1997) 51, arXiv: [hep-ph/9610490](#).
- [45] A. Kulesza and L. Motyka, *Threshold resummation for squark-antisquark and gluino-pair production at the LHC*, *Phys.Rev.Lett.* **102** (2009) 111802, arXiv: [0807.2405 \[hep-ph\]](#).
- [46] A. Kulesza and L. Motyka, *Soft gluon resummation for the production of gluino-gluino and squark-antisquark pairs at the LHC*, *Phys.Rev.* **D80** (2009) 095004, arXiv: [0905.4749 \[hep-ph\]](#).
- [47] W. Beenakker et al., *Soft-gluon resummation for squark and gluino hadroproduction*, *JHEP* **12** (2009) 041, arXiv: [0909.4418 \[hep-ph\]](#).
- [48] W. Beenakker et al., *Squark and gluino hadroproduction*, *Int.J.Mod.Phys.* **A26** (2011) 2637, arXiv: [1105.1110 \[hep-ph\]](#).
- [49] H.-L. Lai et al., *New parton distributions for collider physics*, *Phys.Rev.* **D82** (2010) 074024, arXiv: [1007.2241 \[hep-ph\]](#).



- [50] ATLAS Collaboration, *ATLAS Pythia8 tunes to 7 TeV data*, ATL-PHYS-PUB-2014-021, 2014, URL: <http://cds.cern.ch/record/1966419>.
- [51] T. Gleisberg et al., *Event generation with SHERPA 1.1*, *JHEP* **02** (2009) 007, arXiv: [0811.4622 \[hep-ph\]](#).
- [52] G. Corcella et al., *HERWIG 6: An Event generator for hadron emission reactions with interfering gluons (including supersymmetric processes)*, *JHEP* **01** (2001) 010, arXiv: [hep-ph/0011363](#).
- [53] LHC Higgs Cross Section Working Group, *Handbook of LHC Higgs Cross Sections: 2. Differential Distributions*, CERN-2012-002 (CERN, Geneva, 2012), arXiv: [1201.3084 \[hep-ph\]](#).
- [54] L. Lönnblad and S. Prestel, *Matching Tree-Level Matrix Elements with Interleaved Showers*, *JHEP* **03** (2012) 019, arXiv: [1109.4829 \[hep-ph\]](#).
- [55] W. Beenakker, R. Hopker and M. Spira, *PROSPINO: A Program for the production of supersymmetric particles in next-to-leading order QCD*, (1996), arXiv: [hep-ph/9611232 \[hep-ph\]](#).
- [56] M. Krämer et al., *Supersymmetry production cross sections in pp collisions at  $\sqrt{s} = 7$  TeV*, (2012), arXiv: [1206.2892 \[hep-ph\]](#).
- [57] ATLAS Collaboration, *Modelling of the  $t\bar{t}H$  and  $t\bar{t}V$  ( $V = W, Z$ ) processes for  $\sqrt{s} = 13$  TeV ATLAS analyses*, ATL-PHYS-PUB-2015-022, 2016, URL: <http://cds.cern.ch/record/2120826>.
- [58] ATLAS Collaboration, *Multi-Boson Simulation for 13 TeV ATLAS Analyses*, ATL-PHYS-PUB-2016-002, 2016, URL: <http://cds.cern.ch/record/2119986>.
- [59] D. de Florian et al., *Handbook of LHC Higgs Cross Sections: 4. Deciphering the Nature of the Higgs Sector*, (2016), arXiv: [1610.07922 \[hep-ph\]](#).
- [60] J. Pumplin et al., *New generation of parton distributions with uncertainties from global QCD analysis*, *JHEP* **07** (2002) 012, arXiv: [hep-ph/0201195](#).
- [61] T. Gleisberg and S. Höche, *Comix, a new matrix element generator*, *JHEP* **12** (2008) 039, arXiv: [0808.3674 \[hep-ph\]](#).
- [62] F. Cascioli, P. Maierhofer and S. Pozzorini, *Scattering Amplitudes with Open Loops*, *Phys. Rev. Lett.* **108** (2012) 111601, arXiv: [1111.5206 \[hep-ph\]](#).
- [63] S. Schumann and F. Krauss, *A Parton shower algorithm based on Catani-Seymour dipole factorisation*, *JHEP* **03** (2008) 038, arXiv: [0709.1027 \[hep-ph\]](#).
- [64] S. Höche et al., *QCD matrix elements + parton showers: The NLO case*, *JHEP* **04** (2013) 027, arXiv: [1207.5030 \[hep-ph\]](#).
- [65] D. J. Lange, *The EvtGen particle decay simulation package*, *Nucl. Instrum. Meth.* **A462** (2001) 152.
- [66] ATLAS Collaboration, *Summary of ATLAS Pythia 8 tunes*, ATL-PHYS-PUB-2012-003, 2012, URL: <http://cdsweb.cern.ch/record/1474107>.
- [67] A. D. Martin et al., *Parton distributions for the LHC*, *Eur. Phys. J.* **C63** (2009) 189, arXiv: [0901.0002 \[hep-ph\]](#).

- [68] ATLAS Collaboration, *Vertex Reconstruction Performance of the ATLAS Detector at  $\sqrt{s} = 13$  TeV*, ATL-PHYS-PUB-2015-026, 2015, URL: <https://cds.cern.ch/record/2037717>.
- [69] ATLAS Collaboration, *Electron efficiency measurements with the ATLAS detector using the 2015 LHC proton-proton collision data*, ATLAS-CONF-2016-024, 2016, URL: <http://cds.cern.ch/record/2157687>.
- [70] ATLAS Collaboration, *Muon reconstruction performance of the ATLAS detector in proton-proton collision data at  $\sqrt{s} = 13$  TeV*, *Eur. Phys. J. C* **76** (2016) 292, arXiv: 1603.05598 [hep-ex].
- [71] M. Cacciari, G. P. Salam and G. Soyez, *The anti-kt jet clustering algorithm*, *JHEP* **04** (2008) 063, arXiv: 0802.1189 [hep-ph].
- [72] ATLAS Collaboration, *Topological cell clustering in the ATLAS calorimeters and its performance in LHC Run 1*, (2016), arXiv: 1603.02934 [hep-ex].
- [73] ATLAS Collaboration, *Jet Calibration and Systematic Uncertainties for Jets Reconstructed in the ATLAS Detector at  $\sqrt{s} = 13$  TeV*, ATL-PHYS-PUB-2015-015, 2015, URL: <http://cds.cern.ch/record/2028594>.
- [74] ATLAS Collaboration, *Tagging and suppression of pileup jets with the ATLAS detector*, ATLAS-CONF-2014-018, 2014, URL: <https://cds.cern.ch/record/1700870>.
- [75] ATLAS Collaboration, *Performance of b-Jet Identification in the ATLAS Experiment*, *JINST* **11** (2016) P04008, arXiv: 1512.01094 [hep-ex].
- [76] ATLAS Collaboration, *Expected performance of the ATLAS b-tagging algorithms in Run-2*, ATL-PHYS-PUB-2015-022, 2015, URL: <http://cds.cern.ch/record/2037697>.
- [77] ATLAS Collaboration, *Optimisation of the ATLAS b-tagging performance for the 2016 LHC Run*, ATL-PHYS-PUB-2016-012, 2016, URL: <https://cds.cern.ch/record/2160731>.
- [78] ATLAS Collaboration, *Measurements of the photon identification efficiency with the ATLAS detector using  $4.9 \text{ fb}^{-1}$  of pp collision data collected in 2011*, ATLAS-CONF-2012-123, 2012, URL: <https://cds.cern.ch/record/1473426>.
- [79] ATLAS Collaboration, *Performance of missing transverse momentum reconstruction for the ATLAS detector in the first proton-proton collisions at  $\sqrt{s} = 13$  TeV*, ATL-PHYS-PUB-2015-027, 2015, URL: <http://cds.cern.ch/record/2037904>.
- [80] ATLAS Collaboration, *Expected performance of missing transverse momentum reconstruction for the ATLAS detector at  $\sqrt{s} = 13$  TeV*, ATL-PHYS-PUB-2015-023, 2015, URL: <http://cds.cern.ch/record/2037700>.
- [81] ATLAS Collaboration, *Data-Quality Requirements and Event Cleaning for Jets and Missing Transverse Energy Reconstruction with the ATLAS Detector in Proton-Proton Collisions at a Center-of-Mass Energy of  $\sqrt{s} = 7$  TeV*, ATLAS-CONF-2010-038, 2010, URL: <https://cds.cern.ch/record/1277678>.
- [82] G. Aad et al., *Search for supersymmetry at  $\sqrt{s} = 8$  TeV in final states with jets and two same-sign leptons or three leptons with the ATLAS detector*, *JHEP* **06** (2014) 035, arXiv: 1404.2500 [hep-ex].
- [83] ATLAS Collaboration, *Search for supersymmetry using events with three leptons, multiple jets, and missing transverse momentum in  $13.0 \text{ fb}^{-1}$  of pp collisions with the ATLAS detector at  $\sqrt{s} = 8$  TeV*, ATLAS-CONF-2012-151, 2012, URL: <https://cds.cern.ch/record/1493490>.

- [84] M. Baak et al., *HistFitter software framework for statistical data analysis*,  
*Eur. Phys. J. C* **75** (2015) 153, arXiv: [1410.1280 \[hep-ex\]](#).
- [85] G. Cowan et al., *Asymptotic formulae for likelihood-based tests of new physics*,  
*Eur. Phys. J. C* **71** (2011) 1554, [Erratum: *Eur. Phys. J. C* **73** (2013) 2501],  
arXiv: [1007.1727 \[physics.data-an\]](#).
- [86] A. L. Read, *Presentation of search results: the  $CL_s$  technique*,  
*Journal of Physics G: Nuclear and Particle Physics* **28** (2002) 2693.
- [87] ATLAS Collaboration, *Search for new phenomena in final states with large jet multiplicities and missing transverse momentum with ATLAS using  $\sqrt{s} = 13$  TeV proton-proton collisions*,  
*Phys. Lett. B* **757** (2016) 334, arXiv: [1602.06194 \[hep-ex\]](#).
- [88] ATLAS Collaboration,  
*Search for pair production of gluinos decaying via stop and sbottom in events with b-jets and large missing transverse momentum in pp collisions at  $\sqrt{s} = 13$  TeV with the ATLAS detector*, (2016),  
arXiv: [1605.09318 \[hep-ex\]](#).
- [89] ATLAS Collaboration, *Summary of the searches for squarks and gluinos using  $\sqrt{s} = 8$  TeV pp collisions with the ATLAS experiment at the LHC*, *JHEP* **10** (2015) 054,  
arXiv: [1507.05525 \[hep-ex\]](#).

## Appendix

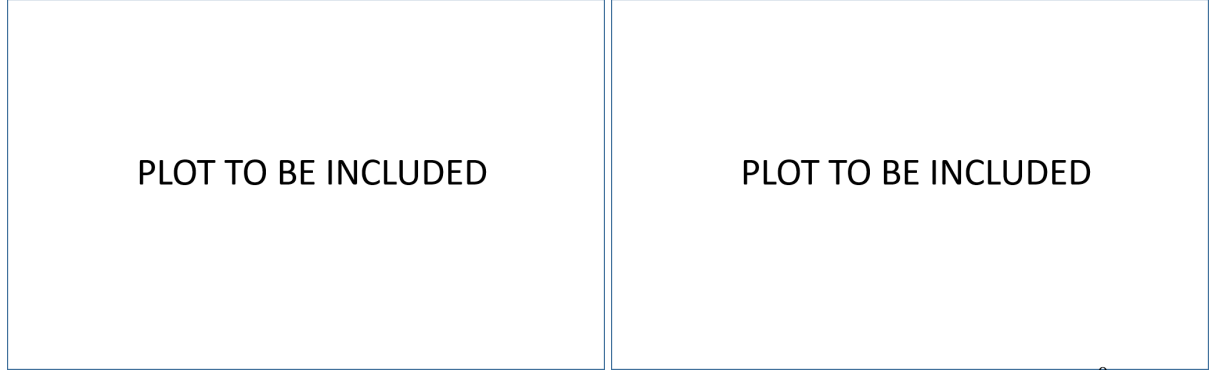


Figure 8: Illustration of the best expected signal region per signal grid point for the  $\tilde{g} \rightarrow q\bar{q}(\ell\ell/\nu\nu)\tilde{\chi}_1^0$  (left) and  $\tilde{g} \rightarrow q\bar{q}'WZ\tilde{\chi}_1^0$  (right) models. This mapping is used for the final combined exclusion limits.

	Raw events	Number of events expected for 36.0fb <sup>-1</sup>
XXX, $\tilde{g} \rightarrow q\bar{q}(\ell\ell/\nu\nu)\tilde{\chi}_1^0$ , $m_{\tilde{g}} = 1.4$ TeV, $m_{\tilde{\chi}_1^0} = 1.1$ TeV		
produced		--
$\geq 3$ leptons ( $p_T > 20, 20, 10$ GeV)		-- $\pm$ --
trigger		-- $\pm$ --
no $b$ -jet ( $p_T > 20$ GeV)		-- $\pm$ --
$\geq 4$ jets ( $p_T > 40$ GeV)		-- $\pm$ --
$E_T^{\text{miss}} > 150$ GeV		-- $\pm$ --

Table 6: Number of signal events selected at different stages of the Signal region definitions, for some of the RPC benchmark scenarios shown on Fig. 1. Only the statistical uncertainties are displayed.

XXXX, $\tilde{g} \rightarrow tds$ , $m_{\tilde{g}} = 1.4$ TeV, $m_{\tilde{t}_1} = 600$ GeV	
produced	--
$\geq 3$ leptons ( $p_T > 20, 20, 10$ GeV)	-- $\pm$ --
trigger	-- $\pm$ --
$\geq 1$ $b$ -jet ( $p_T > 20$ GeV)	-- $\pm$ --
$\geq 6$ jets ( $p_T > 50$ GeV)	-- $\pm$ --
$m_{\text{eff}} > 1.8$ TeV	-- $\pm$ --

Table 7: Number of signal events selected at different stages of the RPV SUSY scenario definitions, for some of the RPV benchmark scenarios shown on Fig. 1. Only the statistical uncertainties are displayed.